Journal of Materials Chemistry A

Accepted Manuscript

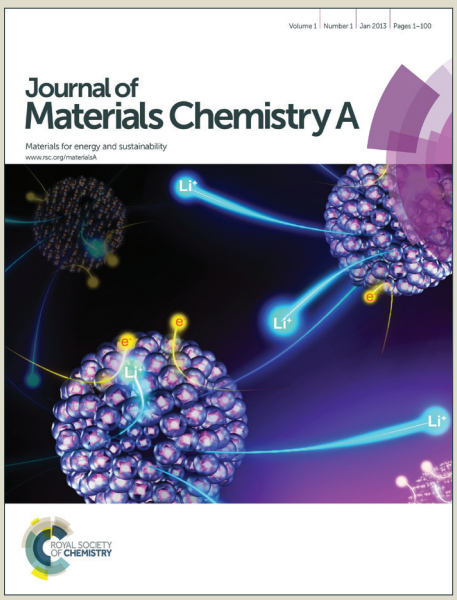

ROYAL SOCIETY OF CHEMISTRY

www.rsc.org/materialsA

Zero-Periodic Metal-Organic Material, Organic Polymer Composites: Tuning Properties of Methacrylate Polymers via Dispersion of Dodecyloxy-Decorated Cu-BDC Nanoballs

Mu-Seong Kim[a], John Perry IV[a], Tamalia C. M. Julien[a], Elisa Marangon[b], Cedric Marrouat[c], Jarrod F. Eubank[d] and Julie P. Harmon[a] *

[a]Department of Chemistry, University of South Florida, 4202 E. Fowler Avenue, Tampa, FL 33620-5250, USA Tel: 1-813-974-3397; fax: 1-813-974-1733.

[b]University of Genova, Via Dodecaneso, 31, 16146 Genova

[c] Ecole Nationale Superieure De Chimie De Clermont Ferrand, Ensemble Scientifique des Cézeaux 24, avenue des Landais BP 1018F – 63174 Aubière Cedex

[d] Department of Chemistry and Physics, Florida Southern College, 111 Lake Hollingsworth Drive, Lakeland, FL 33801

*Correspondence Email: harmon@usf.edu (J.P. Harmon)

Abstract

A self-assembled metal-organic polyhedron (i.e., MOP or nanoball) with $-OC_{12}$ external/surface functionality has been incorporated into two polymeric systems: poly(2-hydroxyethyl methacrylate) (PHEMA) and poly(methyl methacrylate) (PMMA). The nanoball, having the chemical formula $[(DMSO)(MeOH)Cu_2(5\text{-}(dodecyloxy)\text{-}1,3\text{-}benzenedicarboxylate)_2]_{12}$, possesses 24 saturated 12-carbon chains on the surface. This work characterizes the interactions between OC_{12}-decorated nanoballs and the polymers, revealing interesting effects from the polymer perspective. The resultant nanocomposites were characterized by differential scanning calorimetry (DSC) and microindentation. The dielectric permittivity (ε′) and loss factor (ε″) were measured via dielectric analysis (DEA) in the frequency range 1Hz to 100 kHz. The electric modulus formalism was used to

reveal α, β, γ and conductivity relaxations. The nanoball interactions with the different polymer matrices allows for tuning of mechanical and electrical properties, by varying polymer structure and/or nanoball loadings, which could be of interest in applications related to electrochemistry, implantable polymeric sensors, drug delivery, energy storage, and beyond.

Keywords: metal-organic polyhedra, methacrylate polymer nanocomposites, dielectric analysis, microhardness, differential scanning calorimetry

1. Introduction

Polymer composites containing nano-sized fillers have generated an explosive interest since the early 1980's [1-4]. Many recent studies have been conducted incorporating nano-fillers into polymer matrices to design materials with tunable mechanical, thermal, optical, and electrochemical properties [5-13], among others. Conventional filled polymers, where the reinforcement is on the order of microns, have been replaced by composites with discrete nano-sized fillers [14-16]. Gradually, theories predicting composite properties are independent of particle size in the micron range were challenged by nanocomposite data [6]. Nanocomposite properties are greatly influenced by the surface area of the particles and by quantum effects encountered in nanodimensional systems [7]. All of this is complicated by the fact that nanoparticles are inclined to aggregate or migrate to interfaces. Much effort has been devoted to optimize dispersion of nano-fillers in polymer matrices, as polymer-nanoparticle interactions and adhesion greatly influence performance of the material [17,18]. Well-dispersed composites with noncovalent interactions, such as those arising from hydrogen bonding, electrostatic attractions, and π-π interactions [19-21], between the filler and the matrix can transfer stress, and the interface will stop the development of cracks and diminish stress concentrations [22]. Overall, large reinforcement increases are noted at low nanoparticle loadings. Additionally, functional properties, such as thermal and electrical conductivity, porosity, and luminescence, can be tailored for specific applications, such as energy storage [10-13], drug delivery [23], electrochemical implantable biosensors [24], etc. The design of high performance composites requires optimizing dispersion, nanoparticle-polymer noncovalent interactions, and the chemistry of the materials.

Nanocomposites can be grouped in several different ways. For example, Keledi et al. classify nanocomposites according to dimensionality: plates, nanotubes and fibers, and spheres [25]. Hine et al. distinguish between self-reinforcing nanocomposites, where the polymer serves as both reinforcement and matrix, and conventional composites containing hetero-particles [26]. Gacitua et al. reviewed natural and synthetic nanocomposites, and stressed the importance of developing new technologies to mix nano-fillers and polymers on the atomic scale [17]. From a chemistry standpoint, nano-reinforcements are classified as metals, nonmetals, organics, and metal-organics. This study presents a snapshot of some of the swiftly emerging research on (metal-organic material)-polymer nanocomposites and studies conducted in our laboratories.

Metal-organic materials (MOMs) represent a broad class of materials that are very attractive for use in the design of polymer composites. They offer limitless diversity in composition and structure (as well as type and amount of charge), they are easily synthesized via self-assembly, and they are easily processed into nanocomposite materials. Importantly, many are cost effective. MOM structures can be designed to interact with a variety of polymers to produce materials for specific applications.

MOMs, composed of metals or multi-metal clusters and bridging organic ligands are often classified by periodicity [27]. The simplest are discrete, zero periodic structures, such as metal-organic polyhedra (MOPs), some known as nanoballs (NBs), and metal-organic polygons. More extended structures are coordination polymers with periodicity in one, two and three dimensions, sometimes referred to as 1D, 2D and 3D, but more accurately as 1-, 2-, and 3-periodic. Chains, ladders, and tapes are examples of 1D structures. Sheets or bilayers are often classified as 2D structures. The last category, 3D structures, often referred to as metal-organic frameworks (MOFs), is more complex, with some possessing nanometer-sized (or larger) cavities that have the potential to sequester, or adsorb small molecules [28-29], or even encapsulate larger molecules.[30,31]

Many 3D MOFs are permanently porous solids with exceptionally high surface areas. There has been a growing interest in these MOFs for use in applications requiring host-guest chemistry, such as gas storage (including hydrogen and methane for energy applications), drug delivery, catalysis, and chemical separations, and as platforms for nanoscale processes [32-38]. Several interesting studies have also emerged in the area of

MOF-polymer composites [39-44]. Our group was one of the first to study the drug delivery potential of MOF-polymer composites, using a composite made from a zeolite-*like* metal–organic framework, **rho**-ZMOF-1, dispersed in a hydrogel, using 2-hydroxyethyl methacrylate (HEMA), 2,3-dihydroxypropyl methacrylate (DHPMA), N-vinyl-2-pyrolidinone (VP) and ethylene glycol dimethacrylate (EGDMA), where the corresponding release of the anti-arrhythmic drug, procainamide, was analyzed [23].

2D metal-organic structures may also be of interest in composites, as their properites can mimic some clays, in that they may intercalate guest molecules [45]. Organic monomer guest molecules have been incorporated into the structures and then polymerized to form layered structures. The MOM can be removed (usually by degradation), leaving unique organic polymers with interesting matrices containing ordered slits [46,47].

Noteworthy 1D metal-organic architectures have also been synthesized, including helices, zigzag chains, molecular ladders, and nanotubes [45, 48, 49]. In fact, our group of collaborators has previously synthesized a 1-dimensional coordination polymer, copper-4,40-trimethylenedipyridine (Cu-TMDP) [50], which was utilized to prepare a series of poly(methyl methacrylate) (PMMA)/ (Cu-TMDP) composites. Raman characterization led to the conclusion that there is a weak interaction (van der Waals interaction) between the pyridine ring structure and the PMMA matrix. The interaction was manifested in the glass transition temperatures, hardness, and moduli, and increased with Cu-TMDP concentration.

Discrete (0-periodic), nanometer-scale metal-organic structures are also currently of great interest [27,45,51-53]. For one, they are used as building blocks to form higher order network structures. They contain windows allowing them to act as hosts for guest molecules in applications involving drug delivery, separation, sorption, and sensing. Functional groups are varied to produce a diverse array of chemistries, in both the interior and exterior of the structures. Of particular interest, these structures are typically soluble in a variety of organic solvents.

Our group is especially interested in MOP- or NB-polymer composites. NBs resemble rhombihexahedra with the formula $[L_2Cu_2(5\text{-R-bdc})_2]_{12}$ (L = solvent or substituted pyridine, 5-R-bdc = 5-substituted-benzene-1,3-dicarboxylate) [54]. For initial

studies [55,56], we chose a nanoball with hydroxyl functionality: $[(DMSO)(MeOH)Cu_2(5\text{-OH-benzene-1,3-dicarboxylate})_2]_{12}$. This nanoball, referred to as the hydroxyl-NB, has –OH groups on the surface and an internal volume of ~1 nm^3. The square windows have sides 12.749 Å long, and the triangular windows have sides 12.716 Å long. Since MeOH ligands actively bind to the interior surface, it was logical that hydroxyethyl methacrylate (HEMA) could act as a ligand as well, and find its way into the interior of the nanoball. We synthesized a series of PHEMA-nanoball composites, *in situ*, as well as PMMA-nanoball composites. It was anticipated that the PMMA composites would have minimal interactions with the nanoballs as compared to PHEMA. Unlike PMMA, both PHEMA and the nanoballs are soluble in methanol. We probed relaxation dynamics in both sets of composites. PHEMA composites exhibited persistent interactions with the nanoballs, in contrast to the PMMA composites, in which the nanoballs leached from the matrix when immersed in methanol. K. McCann et al. studied interactions of PHEMA, PDHPMA (2,3-dihydroxypropyl methacrylate), and HEMA/DHPMA copolymers with OH-nanoballs [57]. DHPMA decreased the solubility of the nanoball in the polymer matrix, and this, in turn, influenced relaxation behavior.

The synthesis of an alkyl-modified HO-NB, specifically a (dodecyloxy-BDC)-Cu nanoball (OC_{12}-NB), has also been reported [58,59]. This nanoball attracted our interest because the nonpolar dodecyloxy chains offer a hydrophobic environment for interactions with PMMA and PHEMA, in contrast to the hydroxyl-NB mentioned above [55,56]. OC_{12}-NB self-assembles, and the solid structure is $[L_2Cu_2(OC_{12}\text{-bdc})_2]_{12}$ [$(OC_{12}\text{-bdc})_2$ =5-(dodecyloxy)-1,3-benzenedicarboxylate; L = solvent]. In the solid state, the crystal packing is such that each OC_{12}-NB is surrounded by four others in a distorted tetrahedral arrangement (Figure 1). Depending on the solvent and the method used for crystallization, some of the OC_{12} chains may thread through the windows of adjacent OC_{12}-NB molecules [58,59].

Herein, a series of PMMA-(OC_{12}-NB) and PHEMA-(OC_{12}-NB) composites are synthesized *in situ* and characterized using various polymer techniques. The dodecyl groups significantly alter the solubility of the nanoballs, imparting hydrophobicity to the surface of the nanoball. PMMA and PHEMA have different affinities for OC_{12}-NBs. Structure-property relations are discussed in terms of interactions between the polymer

matrices and nanoball surfaces and interiors. Results from this study are compared to our earlier results using OH-nanoballs, wherein we found that variation of basic nanocomposite properties directly correlated with nanoball concentration [55,56]. In designing this experiment, we were particularly interested in documenting the effect of the OC_{12} chain on how properties varied with NB loading. Herein, we characterize glass transition temperatures, microhardness, and dielectric properties. Dielectric analysis (DEA) is a technique that is well-suited for the study of methacrylate polymers, since they have a tendency to exhibit transitions that overlap as the testing frequency increases. In the past, we found that DEA is highly efficient in resolving molecular motion and structural relaxations, as well as in determining the mobility of ions, or ionic conductivity, through PHEMA matrices, which could be of interest in certain energy applications [10-12]. It should be noted that we were the first group to successfully characterize the broad spectrum behavior of PHEMA via DEA [60]. In addition, our reports on the (OC_{12}-NB)- and (hydroxyl-NB)-polymer composites are the first studies, to date, that probe relaxations and conductivity in discrete (metal-organic polyhedra)-polymer composites.

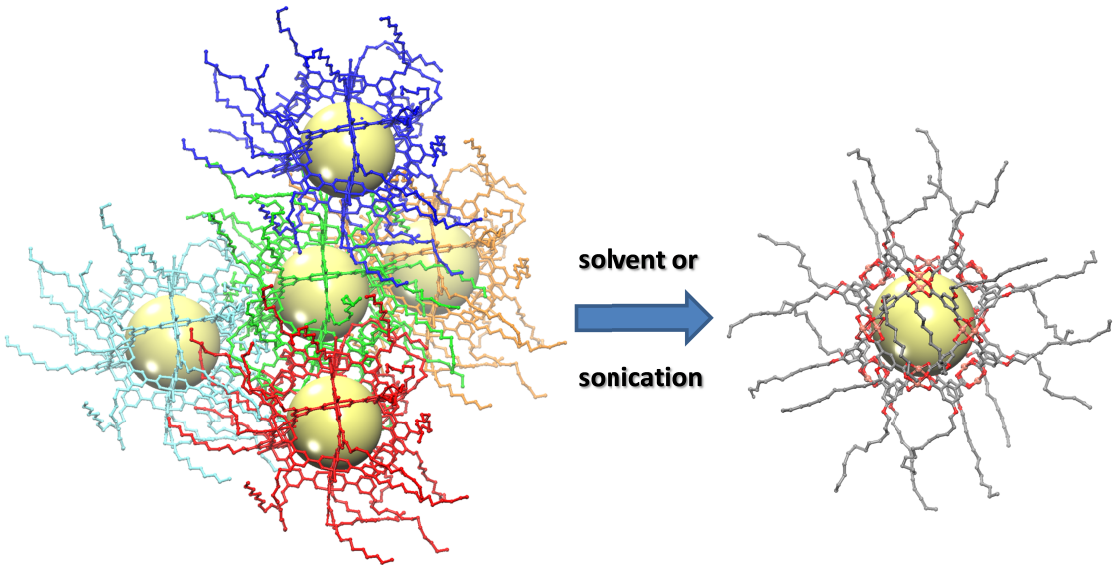

Figure 1. (Left) OC_{12}-NBs pack in a tetrahedral fashion (each NB is represented by a different color, van der Waals sphere represented in yellow). (Right) The 3-periodic

structure can be disrupted upon ultrasonication or exposure to certain solvents to give individual dispersed NBs. [58,59].

2. Experimental

2.1. Materials

Benz R&D (Sarasota, FL) provided 2-hydroxyethyl methacrylate (HEMA) with monomethyl ether hydroquinone (MEHQ) inhibitor removed. Methyl methacrylate (MMA) monomer was purchased from Sigma Aldrich (Milwaukee, WI). The monomethyl ether hydroquinone (MEHQ) inhibitor was removed from the MMA using a fresh MEHQ inhibitor remover column available from Aldrich (Milwaukee, WI). The free radical initiator 2-2'-azobis(2,4-dimethylvaleronitrile) (Vazo 52®) was purchased DuPont (Wilmington, DE).

2.2. Synthesis of OC_{12}-Nanoballs

The OC_{12}-nanoballs were synthesized and characterized by Zaworotko and co-workers as reported previously [58]. It was prepared by dissolving 0.2mmol of $Cu(NO_3)_2 \bullet 2.5\ H_2O$ and OC_{12}-BDC in methanol to which aniline was added and a blue precipitate was formed. 10ml of the methanol and blue precipitate mixture was added to 10 ml of hexane and was shaken. It was allowed to stand for a number of hours forming a blue hexane layer which was then accumulated and layered over neat dimethyl sulfoxide (DMSO). A solid blue material was amassed by centrifugation and it was washed twice with DMSO [58]. The verification of the integrity of the OC_{12}-NB in the polymer composites was found by using steady state fluorescence of the free ligand [58]. Accordingly, it was estimated that greater than 95% of the OC_{12}-NB remained undamaged upon immobilization. This was based upon the integrated emission intensity of the OC_{12}-NB:polymer composite [58].

2.3. Poly (2-hydroxyethyl methacrylate)-Nanoball Nanocomposites

The hydrophobic OC_{12}-nanoballs have minimal affinity for 2-hydroxyethyl methacrylate, and were dispersed throughout the HEMA via *in situ* ultrasonic polymerization at concentrations ranging from 0, 0.05, 0.1 and 0.5% by weight. Using a Branson Sonifier 450, the monomer and nanoballs were sonicated in an ice bath under a nitrogen atmosphere for 1h. Then, 0.2 wt % of Vazo52® was added to the mixture and sonicated under a nitrogen atmosphere and in an oil bath at 60 °C until the mixture became viscous. The sonicator probe was removed and polymerization was allowed to continue in the heated oil bath for 6 h. The samples were post cured at 110 °C for 4 h.

2.4. Poly (methyl methacrylate)-Nanoball Nanocomposites

Since OC_{12}-nanoballs are soluble in MMA, 0, 0.05, 0.1 and 0.5% by weight of nanoballs were added to the MMA monomer prior to polymerization. 0.2 wt % of the free radical initiator, Vazo 52®, was added to the monomer, degassed with dry N_2 gas and polymerized at 80 °C for 24 hr., followed by a post cure session at 110 °C for 6 h.

2.5. Differential Scanning Calorimetry

A TA Instruments DSC 2920 (Differential Scanning Calorimeter) was used to determine the glass transition temperature, T_g, of polymer nanocomposite series. The previously dried samples (3-10mg) were hermetically sealed in aluminum pans and measurements were carried out under a continuous purge with pure nitrogen. The DSC cell was calibrated with an indium standard. Samples were scanned using a ramp rate of 10 ºC /min to 150 ºC, quench cooled with liquid nitrogen to -150 ºC and then reheated at the same rate. The T_g was taken from the second heating cycle.

2.6. Sample Molding

Samples used for measurement in the DEA were compression molded using a Carver Press equipped with a heating element under pressure at a temperature of 160 ºC for 5 min and then air cooled under pressure to room temperature. DEA samples were molded into rectangular disks with dimensions of 25 x 20 x 1 mm. Molded samples were dried in a vacuum oven at 60 ºC and then stored under vacuum in the presence of phosphorous pentoxide.

2.7. Microhardness

A Leica Vickers Microhardness Tester (VMHT) MOT equipped with a square Vickers indenter, with an angle α between non-adjacent faces of the pyramid of 136º, was used to perform microindentation. The Vickers hardness number (HV) for each sample was determined. The values were taken from the average of 10 indents. A load of 500 g and a dwell time of 10 s were used. Each sample was approximately 1 mm thick and measurements were made at room temperature.

2.8. Dielectric Analysis

Dielectric data were collected using a TA Instruments DEA 2970 (Dielectric Analyzer). The analysis was conducted under helium purge of 700 ml/min from a temperature -150°C to 180 ºC for PMMA sample to 260 ºC for PHEMA sample frequencies range from 1 to 100 kHz. Single surface sensors were used. The sample was heated to 135 ºC to embed the sample into the channels of the single surface sensor and then taken down to cryogenic temperature with liquid nitrogen. A maximum force of 250 N was applied to the sample to achieve a minimum spacing of 0.25 mm. Capacitance and conductance were measured as a function of time, temperature and frequency to obtain the dielectric constant, or permittivity (ε′), the dielectric loss (ε″) and the loss tangent (tan $\delta = \varepsilon'/\varepsilon''$).

3. Results and discussion

3.1. Glass transition temperature and microhardness

The glass transition temperature provides insight into deciphering the primary interaction between the nanoballs and the polymer matrix. The T_gs (Table 1) for neat PMMA and PHEMA are 113.2 ºC and 99.8 ºC respectively. The incorporation of OC_{12}-NBs into the PMMA matrix at levels from 0.05-0.5% did not significantly alter the glass transition temperature of the matrix. This indicates that the OC_{12}-nanoballs did not appear to act as either a plasticizer or to strengthen the matrix. The nanoballs are soluble in PMMA, but interfacial interactions are insufficient to alter the glass transition. However the T_g decreased slowly in PHEMA nanocomposites as the NB concentration increased. At 0.5 wt % the glass transition temperature, dropped by about 7 ºC. This is reasonable as the OC_{12} chains are not drawn to the hydrophilic monomer during polymerization. Interactions between the nanoballs and the matrix are minimal. It is conceivable that the OC_{12} chains tend migrate into the cavity of the nanoball when dispersed in the monomer in an effort to avoid the hydrophilic monomer environment. The decrease in the glass transition temperature indicates that there is lack of adhesion or attraction at the filler-polymer interface [6]. Earlier characterization of the solid state structure of the OC_{12}-NB revealed that crystallizing solvents with increased polarity forced the pendant OC_{12} chains into the interior of the structure [58]. This is in contrast to the hydroxyl-nanoball composites we studied earlier [55,56], where glass transition temperature increased smoothly with increasing concentration when the hydroxyl-NBs were dissolved in HEMA and polymerized. This was attributed to the polymer chains threading into the hydroxyl-nanoballs during polymerization. In PMMA, the hydroxyl-nanoball was insoluble, but consistently decreased the T_g of the PMMA matrix due to a plasticizing effect.

Table.1. Glass transition temperature (ºC) and Vicker Hardness number of polymer composites

Sample	Tg/ºC	Hardness number, HV/MPa
Neat PMMA	113.2	241±2.8
0.05% OC_{12}-NB-PMMA	113.5	240±6.4
0.1% OC_{12}-NB-PMMA	114.4	246±4.8

0.5% OC_{12}-NB-PMMA	112.5	235±11.4
Neat PHEMA	99.8	239±8.9
0.05% OC_{12}-NB-PHEMA	99.6	237±5.7
0.1% OC_{12}-NB-PHEMA	97.6	255±8.3
0.5% OC_{12}-NB-PHEMA	92.5	231±10.8

Hardness (*H*) is a measure of a materials resistance to surface deformation [42-44]. It is reported that T_g is proportional to the cohesive energy density (CED) by the following equation [61].

$$T_g = \frac{2\delta^2}{mR} + C_1 \quad (1)$$

$$H = 1.97\,T_g - 571 \quad (2)$$

Where δ^2 is the CED, m is a parameter that describes the internal mobility of the groups in a single chain, R the gas constant and C_1 is a constant. CED is also the contributing factor in hardness. In fact, the relation between T_g and hardness (*H*) is almost linear in ideal systems (2) [84]. Indeed, our earlier hydroxyl NB studies [55,56] exhibited hardness data that tracked along with the glass transition data. That is, both hardness and glass transition temperature increased with NB concentration in the PHEMA but decreased in the PMMA composites [55,56]. This is expected, since the nanoballs associated with PHEMA, but plasticized PMMA. The OC_{12}-NB composites studied herein displayed more complex behavior, as summarized in table 1 above. In both polymers, the hardness numbers increased from neat polymer to 0.1 % filler and then decreased at the 0.5% level. Such decreases are noted at filler levels where agglomeration occurs [62]. There was no direct correlation with hardness and the glass transition temperatures of the samples.

3.2. Dielectric analysis (DEA)

Both of the polymers and the nanoball used in this study have polar groups that are detected via dielectric analysis. DEA is very sensitive to relaxations in polar polymers. Even weak relaxations, which cannot be detected via other techniques, are discernible with DEA, providing that the structures contain dipoles [63,64]. As material is exposed to

an alternating electric field generated by applying a sinusoidal voltage, alignment of dipoles results in polarization. The capacitance and conductance of the material measured over a range of temperature and frequency are related to the permittivity, ε′, and the loss factor, ε″. The dielectric permittivity represents the extent of dipole alignment and the loss factor measures the energy required to align dipoles or move ions [65]. The complex permittivity, ε*, of a system is defined [63].

$$\varepsilon^* = \varepsilon' - i\varepsilon'' \quad (3)$$

It has been documented [56, 60, 63, 65] that PHEMA and PMMA exhibit two sub-T_g (secondary) relaxations and a primary relaxation associated with the glass transition. The transitions are termed α, β, and γ proceeding from high to low temperature. The α transition corresponds the onset of large scale segmental motion of the main chain. The β relaxation marks the rotation of the ester side group and γ relaxation is associated with the rotation of the hydroxyethyl group in PHEMA and with the methyl group rotation in PMMA [63, 66-67]. Methyl group rotation, of course, is not evidenced via DEA. It is well known that β relaxations for polymethacrylates are strong and appear at the shoulders of α peaks [65]. The dielectric spectra of loss factor versus temperature in for PHEMA and PMMA are shown in figure. 2. The gamma relaxation is clearly evident in the lower temperature area of PHEMA plot. The beta and alpha transitions for PHEMA merge and are obscured by conductivity effects at higher frequencies. The beta relaxations for PMMA in Figure 2 are discernible enough to analyze at lower frequencies (below 1,000 Hz) but merge with the alpha transition at higher frequencies. Data for higher temperatures are analyzed via electric modulus formalism (M), where we look at electric loss modulus (M″), are discussed later (formula 8).

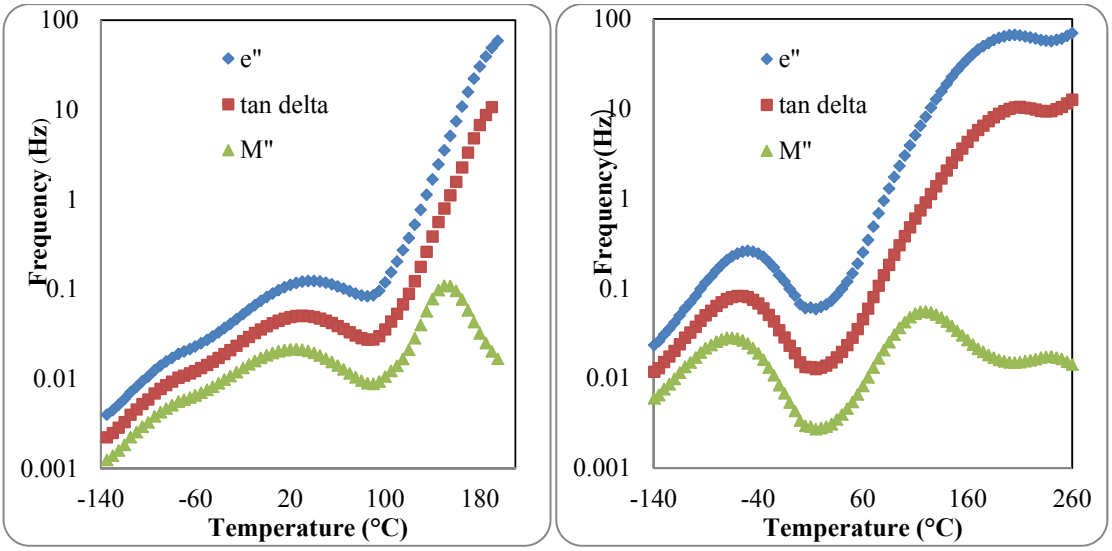

Figure 2. Dielectric loss functions at 100 Hz in (left) neat PMMA and (right) PHEMA

Arrhenius plots of ln frequency vs. reciprocal of temperature for the peak temperature maxima of ε" are linear for secondary transitions [32,49-50]. The slope of an Arrhenius plot is used to determine the activation energies for the PHEMA gamma transition and the PMMA beta transition from:

$$\ln f = \ln f_0 - \frac{\Delta E_a}{RT} \qquad (4),$$

where ΔE_a is the apparent activation energy, R is the gas constant, T is the temperature in Kelvin, f is the frequency, and f_0 is the pre-exponential factor. Such a plot is shown in Figure 3. The activation energies are listed in Table 2.

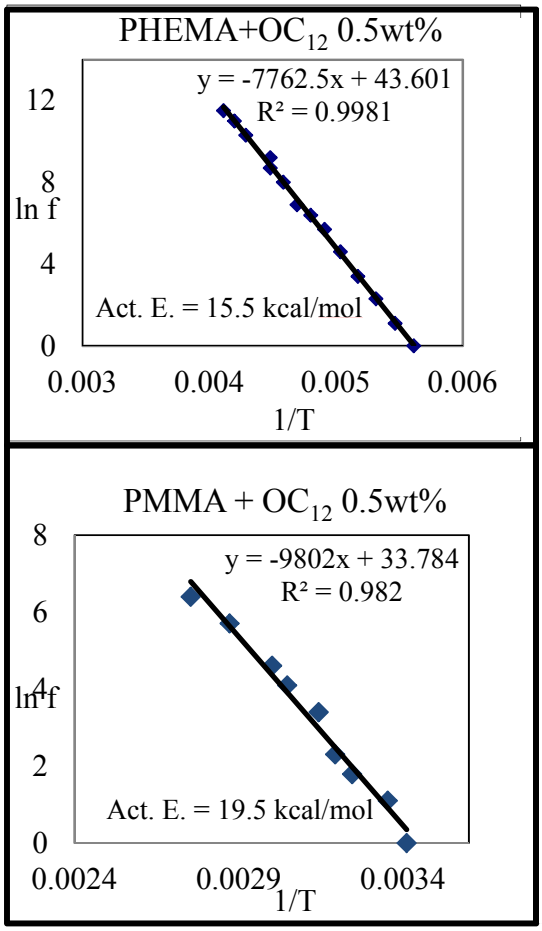

Figure 3. Arrhenius plot of β relaxation for PMMA 0.5 wt% of OC_{12}-composite and γ transition in the PHEMA 0.5wt% of OC_{12}-nanocomposite.

The activation energies for the beta process (ester group rotation) in PMMA-(OC_{12}-NB) composites hardly varied with NB concentration, indicating that the nanoball did not perturb rotation of the side group. By contrast, the hydroxyl-NB plasticized the PMMA matrix and the activation energy for the beta relaxation consistently decreased with NB concentration [56].

Table 2. Activation energies of the β transition for PMMA samples and the γ relaxation in PHEMA samples

Sample	Activation energy/kcal mol^{-1}
Neat PMMA	18.9
0.05% OC_{12}-NB-PMMA	19.2
0.1% OC_{12}-NB-PMMA	19.5
0.5% OC_{12}-NB-PMMA	19.5
Neat PHEMA	18.5
0.05% OC_{12}-NB-PHEMA	17.9
0.1% OC_{12}-NB-PHEMA	17.4
0.5% OC_{12}-NB-PHEMA	15.5

In PHEMA-(OC_{12}-NB) nanocomposites, the activation energy for the gamma transition (hydroxyl group motion) decreased with nanoball concentration for the PHEMA nanocomposites. This indicates that the hydroxyethyl side group rotation is less sterically hindered in the nanocomposites and requires less energy to rotate. Glass transition data revealed that the NB plasticized the PHEMA matrix and this facilitated hydroxyl group alignment in the electric field. This is in contrast to our earlier DEA results for the PHEMA hydroxyl-nanoball composites in that the activation energy for the gamma relaxation increased with nanoball concentration [56]. This was expected, since the hydroxyl-nanoballs are held in the PHEMA matrix with persistent secondary forces.

The dielectric permittivity, ε', increases with the number and strength of the dipoles that align in the electric field. Table 3 shows, as expected, that decreasing the frequency and increasing the temperature facilitate dipole alignment and, ergo, increase ε'. The data reveals that ε' for the PMMA-(OC_{12}-NB) composites decreased slightly with NB concentration. This points to a lack of any significant interactions between the filler and the matrix that would restrict dipole alignment. It also indicates that nonpolar dodecyl group spacers results in a lower dipole density. These minimal changes in ε' with NB concentration follow along with the minimal changes occurring in glass transitions temperatures. The PMMA-(hydroxyl-nanoball) composites exhibited an increase in ε' with

NB content [56]. This agrees with other data discussed above that determined that the hydroxyl-nanoball plasticizes PMMA and allows more effective dipole alignment.

Table 3. Comparison of the dielectric constant, ε', measured at 10 and 1000 Hz for the polymer-nanoball nanocomposites at 25 ºC and 60 ºC.

Sample	ε' @10Hz		ε' @1000Hz	
	25 ºC	60 ºC	25 ºC	60 ºC
Neat PMMA	2.34	2.76	2.05	2.32
0.05% OC_{12}-NB-PMMA	2.34	2.70	2.03	2.30
0.1% OC_{12}-NB-PMMA	2.31	2.70	1.98	2.28
0.5% OC_{12}-NB-PMMA	2.12	2.40	1.81	2.07
Neat PHEMA	5.46	8.81	4.88	8.18
0.05% OC_{12}-NB-PHEMA	5.56	8.87	5.04	8.42
0.1% OC_{12}-NB-PHEMA	5.97	8.93	5.54	8.65
0.5% OC_{12}-NB-PHEMA	7.12	11.2	6.11	10.4

As expected, that ε' is much higher for PHEMA and composites that for the PMMA materials due to the pendant hydroxyl group in PHEMA. The dielectric constant increases with OC_{12} content in PHEMA samples. This points to the fact that the OC_{12} chains may move into NB cavities when sonicated in the HEMA and remain inside after polymerization. This idea arises from the fact that increasing the polarity of solvents for OC_{12}-nanoballs was shown to drive the chains into the interior of the nanoballs [58]. This means that there are less methylene groups on the surface to entangle and deter dipole alignment. It is noteworthy to mention that the hydroxyl-nanoballs were shown to decrease ε' in PHEMA [56]. This was explained by a decrease in dipole alignment due to restricted motion caused by strong secondary interactions between PHEMA and the hydroxyl-NB. Thus, in optimizing dielectric constants, one can design composites with varying dipole strength, matrix mobility and interfacial attractions.

The loss factor term observed in polymeric material contains contributions from two factors. The first factor is the rotational reorientation of the permanent dipoles known

as dipolar relaxation. The second is translational diffusion of ions causing conduction, and this results in a conductivity relaxation that it is possible to discern with proper data analysis [62,68-77]. The contributions to the loss factor are expressed as:

$$\varepsilon'' = \varepsilon''_{dipole} + \varepsilon''_{ion} \quad (5)$$

$$\varepsilon''_{dipole} = (\varepsilon_R - \varepsilon_U)\frac{\omega\tau_E}{1+\omega^2{\tau_E}^2} \quad (6)$$

$$\varepsilon''_{ion} = \frac{\sigma_{ac}}{\omega\varepsilon_0} \quad (7)$$

Where τ_E the dielectric relaxation time, ω is the angular frequency, and ε_R and ε_U represents the low frequency relaxed stat and the high frequency un-relaxed state, respectively.

Conductivity effects are removed by using the electric modulus formalism. In order to obtain the electric modulus, *M*, the mathematical treatment described by Eq. (8) of the complex permittivity, ε*, was carried out by taking the inverse of ε*.

$$M^* = \frac{1}{\varepsilon^*} = M' + iM'' = \frac{\varepsilon'}{(\varepsilon'^2 + \varepsilon''^2)} + \frac{\varepsilon''}{(\varepsilon'^2 + \varepsilon''^2)} \quad (8)$$

M*: complex modulus
M': storage modulus
M": electric loss modulus

Two points are noted after applying electric modulus formalism. First, the maximum in M″ versus temperature plots occurs at a lower temperature than the maxima in tan δ and ε″. Second, although conductivity is a complicating factor, the loss function is minimized because ε′ is present in the denominator to the second power [72].

Figure 2 shows the loss modulus, e″, and electric loss modulus, *M*″, vs. temperature at 10 kHz for the neat samples. The merged beta and alpha relaxation is

clarified in the PHEMA after electric modulus formalism. Figure 4 is shows the plots of M' versus temperature for the PMMA and PHEMA neat and composite samples. The beta transitions were evidenced at frequencies from 1-10 Hz, but merged with the alpha transition at higher frequencies. The beta transition activation energies were calculated from peak heights in M" versus temperature plots and are shown in Table 4. In this set of data, peak maxima were not as clearly discernible as we had noted in our earlier experiments [56]. The data were somewhat scattered, but in the range of values obtained for the PHEMA hydroxyl-NB.

Table 4. Activation energies of the β transition for the PHEMA nanocomposites

Sample	Activation Energy/kcal mol^{-1}
Neat PHEMA	24.6
0.05% OC_{12}-NB-PHEMA	18.3
0.1% OC_{12}-NB-PHEMA	25.3
0.5% OC_{12}-NB-PHEMA	20.5

Electric moduli plots for the PMMA samples demonstrate that at 10 kHz the alpha and beta transitions are nearly completely merged. However, the beta transition activation energies were calculate earlier from e″ values at frequencies < 1,000 Hz since conductivity effects did not interfere with resolution in PMMA, as they do in PHEMA. It is important to note the emergence of a conductivity relaxation peak in both PMMA and PHEMA, neat and composite, samples, as noted in Figure 4. It is well known that space charge effects are suppressed in the electric modulus, and this result in ionic conductivity peaks [72,78-79]. The conductivity peaks for the samples are shown in Figure 4. We believe that this is a conductivity relaxation and not a viscoelastic relaxation. This fact is confirmed by three proofs; Argand plots, ionic translation, and AC conductivity data.

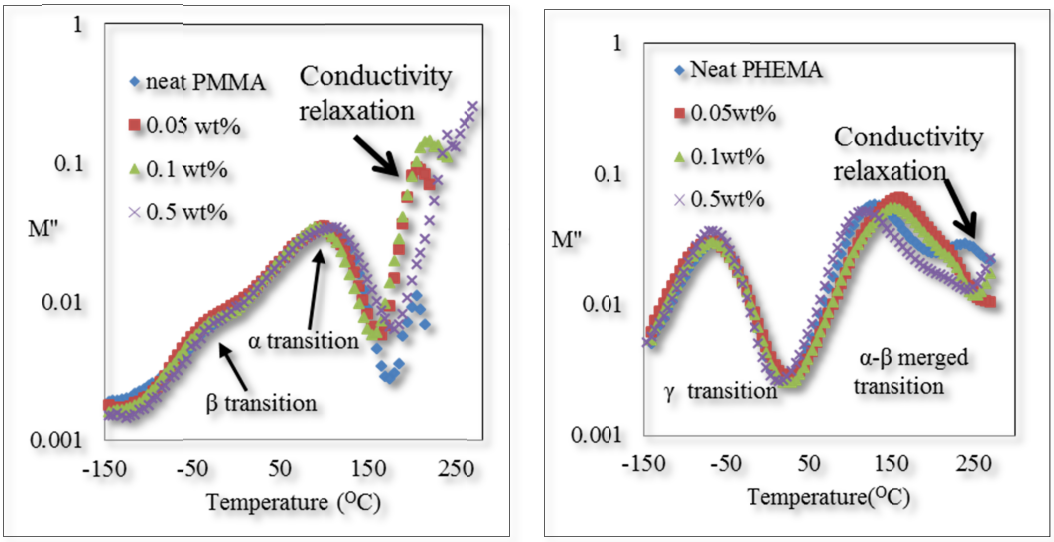

Figure 4. Electric loss modulus (*M″*) vs. temperature at 10 kHz for PMMA and PHEMA neat and composite samples.

Proof 1. Argand plots

In an Argand plot a semi-circular graph is characteristic of the Debye model [80-81,82]. This ideal semi-circle are can be expressed by Debye equation at above *Tg* of polymer, (eq.9) having a single relaxation time.

$$\left(M'\left\{\frac{M_\infty - M_s}{2}\right\}\right)^2 + (M'')^2 = \left(\frac{(M_\infty - M_s)}{2}\right)^2 \qquad (9)$$

M_∞ : Electric Modulus at high frequency ($\omega \to \infty$)
M_s : Electric Modulus at zero frequency ($\omega \to 0$)

Both the PHEMA and PMMA nanocomposite series exhibited semi-circular behavior at temperatures well above the glass transition region where the plots exhibit Debye behavior. Figure 5 shows the Argand plot of neat PHEMA and the series of nanocomposites. On the other hand, in temperature regions over which viscoelastic relaxations occur in Argand plots deviate from semicircular behavior due to a distribution of relaxation times. True semi-circular behavior is interpreted to mean that there are not viscoelastic relaxations with a distribution in relaxation times; they are conductivity relaxations.

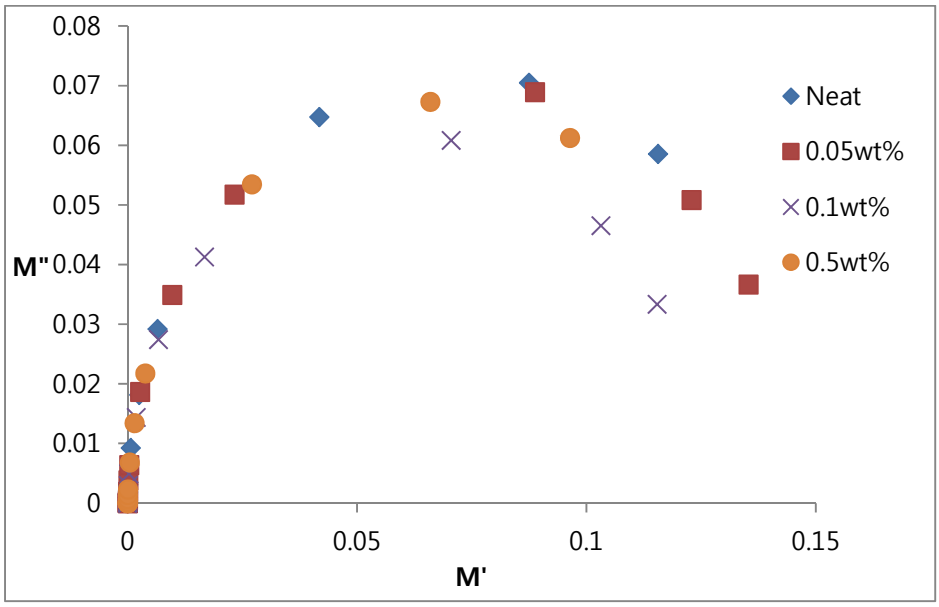

Figure 5. Argand plot derived from the conductivity relaxation region for PHEMA samples (180 ºC).

Proof 2. Log M′ and log M″ vs. Log frequency

The expression for the electric modulus, (M), Eq. (10), was employed under the assumption that ionic conduction results from the diffusion of ions independent of viscoelastic and dipole relaxation in terms of time, frequency and modulus [71-73,75].

$$M = M_s\left(\frac{i\omega\tau_\sigma}{1+i\omega\tau_\sigma}\right)$$

$$= M_s\left[\frac{(\omega\tau_\sigma)^2}{1+(\omega\tau_\sigma)^2}\right] + iM_s\left[\frac{\omega\tau_\sigma}{1+(\omega\tau_\sigma)^2}\right] \qquad (10)$$

In Eq. (10) $M_s = {}^{1}/_{\varepsilon_R}$ where ε_R occurs at a value of ε' that is independent of temperature. It follows from Eq. (10) in this assumption above that plots of log M′ and log M″ vs. log frequency will have slopes of 2 and 1 respectively at low frequency [72,83].

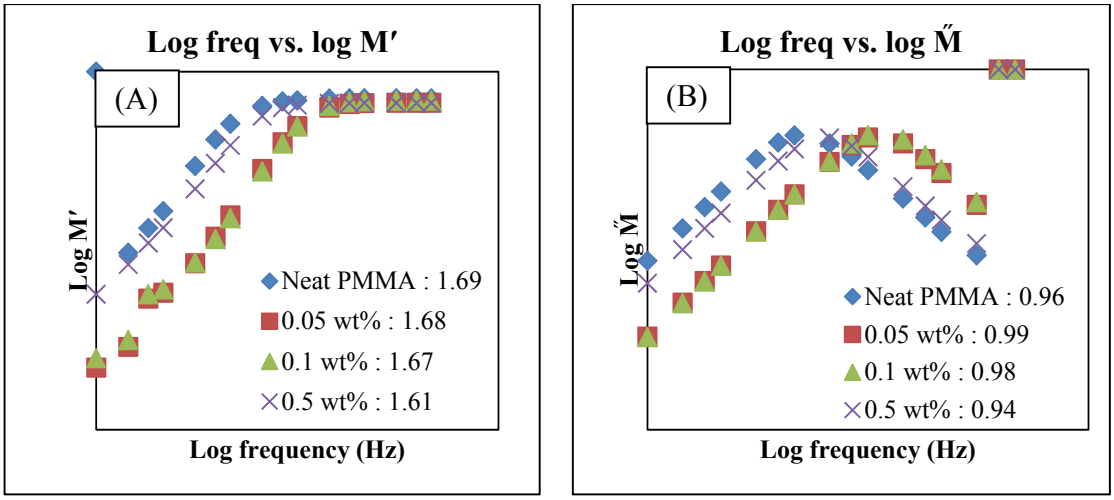

Figure 6. Dependence of M′ and M″ on frequency in the conductivity relaxation region. (a) M′ dependence for PMMA; (b) M″ dependence for PMMA.

Figure 6 shows the plots of log M′ and log M″ vs. log frequency PMMA nanocomposites above the glass transition temperature region. The actual slope value for the M′ and M″ for polymer composites series is shown as an inset in Figure 6. All samples approach the ideal value of 2 for log M′ and 1 for log M″; whereas similar plots were not obtained for temperatures in the glass transition temperature region and below. This result confirmed that the observed relaxations are due to ionic conductivity. Similar results were obtained for the PHEMA series.

Proof 3. AC conductivity

The ionic conductivity was used to further substantiate the above data. The ionic conductivity is related to the movement of ions through the polymer matrix when viscoelastic effects are negligible and AC conductivity, σ_{AC}, is given by the equation:

$$\sigma_{AC} = \acute{\varepsilon}\omega\varepsilon_0 \qquad (11)$$

where ω is the angular frequency and ε_0 is the absolute permittivity of free space (8.854×10^{-12} F/m) [71-72]. The plots for the frequency dependence of AC conductivity (σ_{AC}) in the temperature range above T_g where conductivity is present are shown in Figure 7.

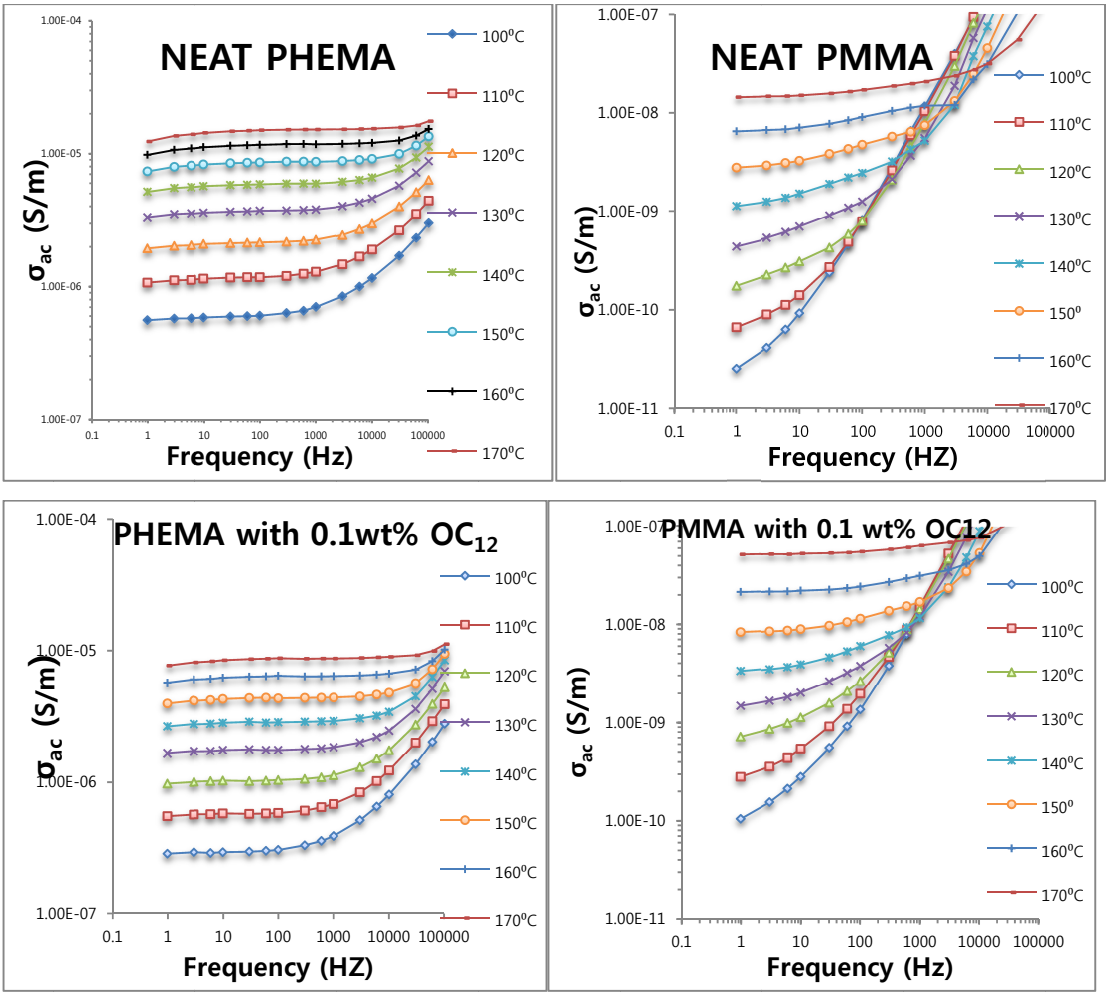

Figure 7. Frequency dependence of ac conductivity for neat PHEMA and neat PMMA and 0.1% composites at temperatures from 100-170 ºC.

The AC conductivity is dependent on frequency at low temperatures. However, the frequency dependence of AC conductivity gradually disappears and plateaus as temperature is increased. This signifies the beginning of the conductivity relaxation region and illustrates the independence of all frequencies measured at high temperature.

Representative values for AC conductivity are shown in Table 5. Overall, neat PHEMA and PHEMA-nanocomposites exhibit greater conductivity than the PMMA series. Conductivities are within the range of those observed in the hydroxyl-nanoball studies [56].

Table.5. Ionic conductivity of the polymer nanocomposites at 160 ºC and 10Hz.

Sample	10Hz (S/m)
Neat PMMA	7.07×10^{-9}
0.05% OC_{12}-NB-PMMA	1.34×10^{-8}
0.1% OC_{12}-NB-PMMA	2.22×10^{-8}
0.5% OC_{12}-NB-PMMA	1.31×10^{-8}
Neat PHEMA	1.12×10^{-5}
0.05% OC_{12}-NB-PHEMA	4.00×10^{-6}
0.1% OC_{12}-NB-PHEMA	6.18×10^{-6}
0.5% OC_{12}-NB-PHEMA	1.66×10^{-5}

Table 6. Ionic conductivity activation energy for PHEMA and PMMA composites

Sample	Activation Energy/ kcalmol-1
Neat PMMA	12.9
0.05% OC_{12}-NB-PMMA	12.6
0.1% OC_{12}-NB-PMMA	12.7
0.5% OC_{12}-NB-PMMA	12.7
Neat PHEMA	7.4
0.05% OC_{12}-NB-PHEMA	7.4
0.1% OC_{12}-NB-PHEMA	6.9
0.5% OC_{12}-NB-PHEMA	6.2

DC conductivity (σ_{DC}) was calculated from the data in Figure 7 by extrapolation to zero frequency. The DC conductivity follows an Arrhenius relationship described by Eq. (12) and activation energy (Table 6) obtained by Eq. (12), where E is the apparent activation energy, k is Boltzmann's constant and σ_0 is the pre-exponential factor [83].

$$\log \sigma_{Dc} = \log \sigma_0 \exp\left(\frac{-E}{kT}\right) \quad (12)$$

Activation energies were obtained from plots of log (σ_{DC}) versus 1/T. The ionic conductivity activation energies, the energies required to bring about the translation diffusion of ions in polymer matrix, were constant in the PMMA series. This is in contrast to earlier results on the hydroxyl-nanoball samples, where activations energies decreased smoothly with nanoball concentrations.

The activations energies for the PHEMA series decreased slightly with the concentration of OC_{12}-nanoballs. This indicates that the nanoballs assisted ions transport, possibly due to a lack of adhesion at the filler-polymer interface. Previous studies with the hydroxyl-nanoball in PHEMA noted an increase in activation energies for conductivity with increasing NB concentration [56]. This was attributed to interactions between the nanoball and PHEMA that impeded motion in the composite. PMMA-(OC_{12}-NB) samples exhibited anomalous behavior.

4. Conclusions

This study characterized the effect of zero-periodic OC_{12}-nanoballs on methacrylate polymer properties. DSC revealed that the NB did not affect the glass transition temperature of PMMA composites, but did decrease the T_g of PHEMA composites. In both matrices, hardness values increased with filler levels up to 0.1 wt% and then decreased, possibly due to agglomeration. Dielectric analysis revealed the expected γ transition in PHEMA samples, which decreased with the addition of NBs, indicating that the nanoball loosens the matrix to ease side group rotation. Dielectric constants, ε's, increased with NB concentration in PHEMA, but slightly decreased with NB concentration in PMMA. In PHEMA, the OC_{12} chains enter the nanoball, and the outside of the nanoball contributes to dipole alignment. In PMMA composites, there are no significant interactions that contribute to dipole alignments, and the hydrocarbon chains on the outside of the nanoball are not dielectrically active. Conductivities were higher in the PHEMA series than in the PMMA series. Activation energies for conductivity were constant for the PMMA series, but decreased slightly with filler loading in the PHEMA series. The electric modulus formalism was used to separate conductivity relaxations from viscoelastic relaxations. Argand plots of M' versus M" revealed a single relaxation time at higher temperatures for all samples, which confirm

conductivity that is not obscured by viscoelastic interference. Overall, we have demonstrated that we were able to characterize both structural and conductivity relaxations throughout broad temperature regions in filled and unfilled polymers. Importantly, the dodecyl appendages on the nanoballs resulted in more scattered data than that obtained in previous studies on hydroxyl-nanoball nanocomposites. Our results support the potential for tuning the properties, including electrochemical properties for applications like energy storage, of polymers via the use/incorporation of newly designed zero-periodic metal-organic polyhedra and/or nanoball structures.

Acknowledgements

The authors would like to thank Dr. Shengqian Ma (University of South Florida) for useful discussions, University of South Florida for undergraduate research support and M. Zaworotko and his group for providing nanoball samples. This work was supported in part by the Department of Defense under grant HDTRA1-08-0035.

References

[1] R. Roy, S. Komarneni and D. M. Roy, *Mater. Res. SOC. Symp. Proc.,* 1984, **32,** 347-359.

[2] Carter, Forrest L., *Superlattices and Microstructures*,1986, 2(2), 113-28.

[3] A. Das, R. Messier, T. R. Gururaja, L. E. Cross, *Materials Research Society Symposium Proceedings*, 1986, **72** (Electron. Packag. Mater. Sci. 2), 27-33.

[4] S. Komarneni, *J. Mater.*, 1992, **2**(12), 1219-1230.

[5] K.J. Kim and M. Shahinpoor, *Smart Mater. Struct*., 2003, **12**, 65-79.

[6] J. Jordan, K.I. Jacob, R. Tannenbaum, M.A. Sharaf, and I. Jasiuk, *Mater. Sci. Eng. A,* 2005, **393**, 1-11.

[7] F. Hussain, M. Hojjati, M. Okamoto and R.E. Gorga, *J. Compos. Mater*., 2006, **40**, 1511-1575.

[8] M. Moniruzzaman and K.I. Winey, *Macromolecules*, 2006, **39**, 5194-5205.

[9] A.S. Kumbhar and G. Chumanov, *Chem. Mater*., 2009, **21**, 2835-2839.

[10] H. Krebs, L. Yang, N. Shirshova, J. H.G. Steinke, *Reactive and Functional Polymers* 2012, **72**(12), 931–938.

[11] A. Gupta, R. H. Liang, S. D. Hong, S. Di Stefano, D. R. Coulter, S. Y. Chung, K. L. Oda, A. K. Clayton, E. Laue, *MiCon 82: Optimization of Processing, Properties, and Service Performance Through Microstructural Control, ASTM STP 792*, H. Abrams, E. Clark, J. Hood, B. Seth, Eds., American Society for Testing and Materials, 1982, pp. 320-339.

[12] L. Pan, G. Yu, D. Zhai, H. R. Lee, W. Zhao, N. Liu, H. Wang, B. C.-K. Tee, Y. Shi, Y. Cui, Z. Bao, *PNAS*, 2012, **109**(24), 9287–9292.

[13] A. Guiseppi-Elie, *Biomaterials* 2012, **31**, 2701–2716.

[14] S.K. Jewrajka, U. Chatterjee, *J. Polym. Sci. Polym. Chem.,* 2006, **44**, 1841-1854.

[15] Y. Shi, Y. Fu, C. Lu, L. Hui and Z. Su, *Dyes and Pigments*, 2010, **85**, 66-72.

[16] S.Bal and S.S. Samal, *Bull. Master. Sci*. 2007, **30**, 379-386.

[17] E.W. Gacitua, A. A. Ballerini and J. Zhang, Maderas. Ciencia y tecnología, 2005, **7** (3), 159-178.

[18] H. Zhang, Y. Liu, D. Yao and B. Yang, *Chem. Soc. Rev*., DOI: 10.1039/c2cs35038f.

[19] A.F.M. Kilbinger and R.H. Grubbs, *Angew. Chem. Int. Ed*., 2002, **41**, 1563-1566.

[20] D. Porter, *Group Interaction Modelling of Polymer Properties*, Marcel Dekker, Inc., New York, 1995, 15-35.

[21] M. Jiang, M. Li, M. Xiang and H. Zhou, *Adv. Polym. Sci*., 1999, **146**, 121-196.

[22] J.Z. Liang, *Polym. Compos*., 2011, **32**, 821–828.

[23] R. Ananthoji, J. F. Eubank, F. Nouar, H. Mouttaki, M. Eddaoudi and J. P. Harmon, *J. Mater. Chem*., 2011, **21**, 9587-9594.

[24] C. Wang, B. Yu, B. Knudsen, J. Harmon, F. Moussy, Y. Moussy, *Biomacromolecules*, 2008, 9(2) 561-567.

[25] G. Keledi, J. Hari and B. Pukanszky, *Nanoscale*, 2012, **4,** 1919-1938.

[26] P. Hine, V. Broome and I. Ward, *Polymer*, 2005, **46** (24) 10936–10944.

[27] J. J. Perry IV, J. A. Perman and M. J. Zaworotko, *Chem. Soc. Rev.,* 2009, **38,** 1400-

1417.

[28] H. Li, M. Eddaoudi, M. O'Keefe and O. M. Yaghi, *Nature*, 1999, **402,** 276-279.

[29] M. Eddoudi, J. Kim, N. Rosi, D. Vodak, J. Wachter and M. O'Keefe, *Science*, 2002, **295,** 469-472.

[30] M. H. Alkordi , Y. Liu, R. W. Larsen , J. F. Eubank and M. Eddaoudi, *J. Am. Chem. Soc.*, 2008, **130** (38), 12639–12641.

[31] Y. Chen, V. Lykourinou, T. Hoang, L.-J. Ming, S. Ma, *Inorg. Chem.*, 2012, **51**, 9156-9158

[32] M. H. Alkordi and M. Eddaoudi, *Supramolecular Chemistry: From Molecules to Nanomaterials*, Eds. P. A. Gale and J. W. Steed, 2012, John Wiley and Sons, LTD, 3-87-3104.

[33] S. Ma and Hong-Cai Zhou, *Chem, Commun,* 2010, **46,** 44-53.

[34] A. R. Millward, and O. M. Yaghi *J. Am. Chem. Soc.*, **2005**, 127 (51), 17998-17999.

[35] P. Horcajada1, T. Chalati, C. Serre1, B. Gillet, C. Sebrie, T. Baati1, J. F. Eubank, D. Heurtaux, P. Clayette, C. Kreuz, Jong-San Chang, Y. K. Hwang, V. Marsaud, Phuong-Nhi Bories, L. Cynober, S. Gil, G. Férey, P. Couvreur and R. Gref, *Nature Materials*, 2010, **10,** 172-178.

[36] J. Y. Lee , O. K. Farha , J. Roberts , K. A. Scheidt , S. T. Nguyen and J. T. Hupp, *Chem. Soc. Rev.,* 2009, **38**, 1450-1459.

[37] D. N. Dybtsev, H. Chun, S. H. Yoon, D. Kim, and K. Kim, *J. Am. Chem. Soc.,* 2004, **126** (1), 32–33.

[38] T. Uemura, N. Yanai and S. Kitigawa, *Chem. Soc. Rev*., 2009, **38,** 1228-1236.

[39] T. Uemura, in Supramolecular Soft Matter; *Applications in Materials and Organic Electronics,* John Wiley & Sons, Hoboken, 2011, pp. 175-189.

[40] H. Yehia, T. J. Pisklak, J. P. Ferraris, K. J. Balkus and I. H. Musselman, *Abstr. Paper Amer. Chem. Soc.,* 2002, 227, U351.

[41] J. A. Thompson, K. W. Chapman, W. J. Koros, C. W. Jones, S. Nair, *Microporous and Mesoporous Materials,* 2012, **158,** 292-299.

[42] R. Adams, C. Carson, J. Ward, R. Tannenbaum and W. Koros*, Microporpous and Mesoporous Materials,* 2010, **131** (103) 13-20.

[43] K. Dawson, A, Mokrini, J. Hurd, and G. K. Shimizu,
From Pacifichem 2010, *International Chemical Congress of Pacific Basin Societies*,
Honolulu, HI, United States, December 15-20, 2010 (2010), AETECH-456.

[44] S. S. Han and W. A. Goddard III, *J. Phys. Chem*., 2007, **111**(42), 15185-15191.

[45] M. J. Zaworotko, *Chem. Commun.,* 2001, 1-9.

[46] N. Yanai, T. Uemura, M. Ohba, Y. Kadowaki, M. Maesato, M. Takenaka, S. Nishitsuji, H. Hasegawa,and S. Kitagawa, *Angewandte Chemie, International Edition*, 2008, **47**(51), 9883-9886.

[47] F. Cui, J. Zhang, T. Cui, B. Li, Q. Lin and B. Yang, *Nano. Res.,* 2008, **1,**195-202.

[48] F. Dai, H. He and S. Sun, *J. Am. Chem. Soc*., 2008, **130,** 14064-14065.

[49] J-T Yu, J. Sun, Z-T. Huang and Q-U. Zheng, *Cryst. Eng. Comm*, 2012, **14,** 112-155.

[50] S. Liu, R. Ananthoji, S. Han, B. Knudsen, X. Li, L. Wojtas, J. Massing, C. Valdez Gauthier and J. P. Harmon, *New J. Chem.,* 2012, **36**, 1449–1456.

[51] M. J. Zaworotko, *Nat. Chem*, 2009, **1,** 267-268.

[52] B. Moulton, J. Lu, A. Monda and M. J. Zaworotko, *Chem. Commun*., 2001, **9**, 863–864.

[53] A. Schaate, P. Roy, A. Godt, J. Lippke, F. Waltz, M. Wiebcke, P. Behrens, *Chem. Eur. J*. 2011, **17**, 6643 – 6651.

[54] H. Abourahma, A.W. Coleman, B.Moulton, B. Rather, P.Shahgaldian and M. J. Zaworotko, *Chem. Commun.,* 2001, **22,** 2380–2381.

[55] K. Mohomed, H. Abourahma, M. J. Zaworotko and J. P. Harmon, *Chem. Commun.*, 2005, 3277-3279.

[56] K. Mohomed, T. Gerasimov, H. Abourahma, M. Zaworotko and J. P. Harmon, *Matls. Sci. and Eng. A*, 2005, **409,** 227-233.

[57] K. McCann, B. Knudsen, R. Ananthoji, B, Hilker, and Julie P. Harmon, *J. Nano. Sci. Tech.*, 2010, **10,** 5557–5569.

[58] J. J. Perry, V. C. Ktavtsov, M. J. Zaworotko and R. W. Larsen*, Cryst. Growth Des,* 2011, **11,** 3183-3189.

[59] H. Furukawa, J. Kim, K.E. Plass and O. M. Yaghi, *J. Am. Chem. Soc.,*2006, **128,** 8398-8399.

[60] K. Mohomed, T. G. Gerasimov, F. Moussy and J. P. Harmon, *Polymer*, 2005, **46**, 3847-3855.

[61] F.J.B. Calleja, S. Fakirov, *Microhardness of Polymers*, Cambridge University Press, New York, 2000, 62-65.

[62] B. Yang, m. LI, . Y. Wu, and X. Wan, *Polymers & Polymer Composites*, 2013, **21** (1)*,* 37-42.

[63] N. G. McCrum, B. E. Read and G. Williams, *An Elastic and Dielectric Effects in Polymeric Solids*, Dover Publication, New York, 1967.

[64] L. Nunez, S. Gomez-Barreiro, C.A. Gracia-Fernandez and M.R. Nunez, *Polymer*, 2004, **45**, 1167–1175.

[65] K. Mohomed, F. Moussy and J. P. Harmon, *Polymer,* 2006, **47**, 3856-3865.

[66] G. Gates, J.P. Harmon, J.Ors and P. Benz, *Polymer,* 2003, **44**, 207-214.

[67] J. Janacek*, J. Macromol. Sci. Rev. M*., 1973, **9**, 1-47.

[68] J. Kolarik, Secondary Relaxations in Glassy Polymers, in : H. J. Cantow (Ed*), Adv. Polym. Sci.*, **46,** Springer-Verlag, 1982, 119-163.

[69] U. W. Gedde, *Polymer Physics*, Chapman & Hall, New York, 1995, 77-97.

[70] J. L. Gomez and R. Diaz, *J. Polym. Sci. Part B: Polym. Phys*., 1985, **23**, 1297-1307.

[71] P. B. Macedo, C. T. Moynihan and R. Bose, *Phys. Chem. Glasses*, 1972, **13**, 171-179.

[72] H.W. Starkweather and P. Avakian, *J. Polym. Sci. Part B: Polym. Phys*., 1992, **30**, 637-641.

[73] G. P. Johari and K. Pathmanathan, *Phys. Chem. Glasses,* 1988, **29**, 219-224.

[74] R. Bergman, F. Alvarez, A. Alegria and J. Colmenero, *J. Chem. Phys*., 1998, **109**, 7546-7555.

[75] J. H. Ambrus, C. T. Moynihan and P. B. Macedo, *J. Phys. Chem*., 1972, **76**, 3287-3295.

[76] Y. Sun, Z. Zhang and C. P. Wong, *Polymer*, 2005, **46**, 2297-2305.

[77] M.S. Kim, P.K. Sekhar, S. Bhansali and J. P. Harmon, *J. Nanosci. Nanotechnol*., 2009, **9**, 5776-5784.

[78] G. M. Tsangaris, G.C. Psarras and N. Kouloumbi, *J mater Sci,* 1998, **33**, 2027-2038.

[79] P. Pissis and A. Kyritsis, *Solid State Ionics,* 1997, **97**, 105-113.

[80] S. K. Emran, G. R. Newkome, C. D. Weis and J. P. Harmon, *J. Polym. Sci. Part B: Polym. Phys*., 1999, **37**, 2025-2038.

[81] J. P. Runt and J. J. Fitzgerald, *Dielectric Spectroscopy of Polymeric Materials*, Oxford University press, Washington DC, 1997.

[82] B. Hilker, K.B. Fields, A. Stern, B. Space, X.P. Zhang and J.P. Harmon, *Polymer,* 2010, **51**, 4790-4805.

[83] P. Avakian, H. W. Starkweather and W. G. Kampert*, in Handbook of Thermal Analysis and Calorimetry* edited S. Z. G. Cheng, Elsevier, New York, 2002, **3**, 147.

[84]S. Farikov, F. J. Balta Calleja and M. Boyanova, *Journal of Material Science Lett*ers, 22, 2003, 1011-1013